DETECTING PULSAR POLARIZATION BELOW 100 MHz WITH THE LWA

Veronica J. Dike[1]

—

Advisors

Dr. Gregory Taylor[1] and Dr. Kevin Stovall[1,2]

[1]*Department of Physics and Astronomy, University of New Mexico*

[2]*National Radio Astronomy Observatory*

ABSTRACT

Pulsars are neutron stars that emit a beam of electromagnetic radiation from their magnetic poles as they spin, creating short, regular pulses. With the first station of the Long Wavelength Array (LWA1), an interferometric radio telescope consisting of 256 dipole antennas, we can study pulsar emission at long wavelengths. Polarized light from pulsars undergoes Faraday rotation as it passes through the magnetized interstellar medium. Observations from LWA1 are ideal for obtaining precise rotation measures (RMs) because the effect of Faraday rotation is proportional to the square of the observing wavelength. With these RMs, we obtained polarized pulse profiles to see how polarization changes in the 10-88 MHz range. Observing at multiple frequencies is important because it can give us insight into the pulsar emission mechanism. RMs are also used to find the electron density weighted average magnetic field along the line of sight. We found rotation measures and polarization profiles of 15 pulsars acquired using data from LWA1. The RMs were used to derive values for the average Galactic magnetic field along the line of sight.

1. INTRODUCTION

1.1. *Pulsars and the Interstellar Medium*

A pulsar is a type of neutron star, an extremely compact object whose main component is densely packed neutrons. Neutron stars were predicted to be a product of supernovae by Baade & Zwicky (1934). The first neutron star to be observed was PSR B1919+21 by Hewish et al. (1968) with a dipole interferometer operating at 81.5 MHz at the Mullard Radio Astronomy Observatory. Because each pulse of this pulsar has a width of less than 0.016 seconds, the source has to be a compact object. As more pulsars were discovered, their properties became clear: they are rapidly rotating, highly magnetized neutron stars that emit beams of radiation as they rotate, which results in the observed regular pulse. Although a small number of neutron stars have been found that do not emit radiation in this manner (see, for example, Klochkov et al. 2013), the overwhelming majority of observable neutron stars are pulsars.

Typical, or 'regular' pulsars rotate with periods of about 100 milliseconds to 10 seconds, while the class of millisecond pulsars, which 'spin up' due to accretion from a binary partner, have periods on the order of a few milliseconds. This rapid rotation combined with degeneracy pressure from the Pauli exclusion principle keep pulsars from collapsing into black holes. The stable rotation of pulsars allows them to be used as tools to study other areas of astrophysics.

One area that can be studied by pulsars is the interstellar medium: the dust and gas between the stars of our Galaxy. One important effect of this medium on pulsar observations is dispersion, which causes an observing frequency dependent delay in the pulse arrival time (See figure 1). This delay is proportional to the square of the observing wavelength and the dispersion measure (DM), which is the electron column density integrated from the observer to the pulsar. Therefore, the measured delay can be used to find a value for the DM. The DM can then be used to find electron density along the line of sight if the distance to the pulsar is known, or vice versa. For any pulsar observation, DM must be found and the pulse must be "de-dispersed" so that the pulse is not smeared out.

1.2. *Polarization*

Pulsar polarization is useful for both the study of pulsars and the study of the Galactic magnetic field. Shortly after the discovery of the first pulsar, Lyne & Smith (1968) established that they are linearly polarized and suggested using a measure of Faraday rotation of the polarized signal to study the magnetic field of the intervening interstellar medium. Faraday rotation is the rotation in the polarization position angle of the source's light as it travels through the magnetized interstellar medium. This rotation occurs because the left- and right-circularly polarized components of the light have different indices of refraction. Faraday rotation is proportional to λ^2. The proportionality constant is the rotation measure (RM), an observable that can be used to derive the component of the magnetic field parallel to the line of sight

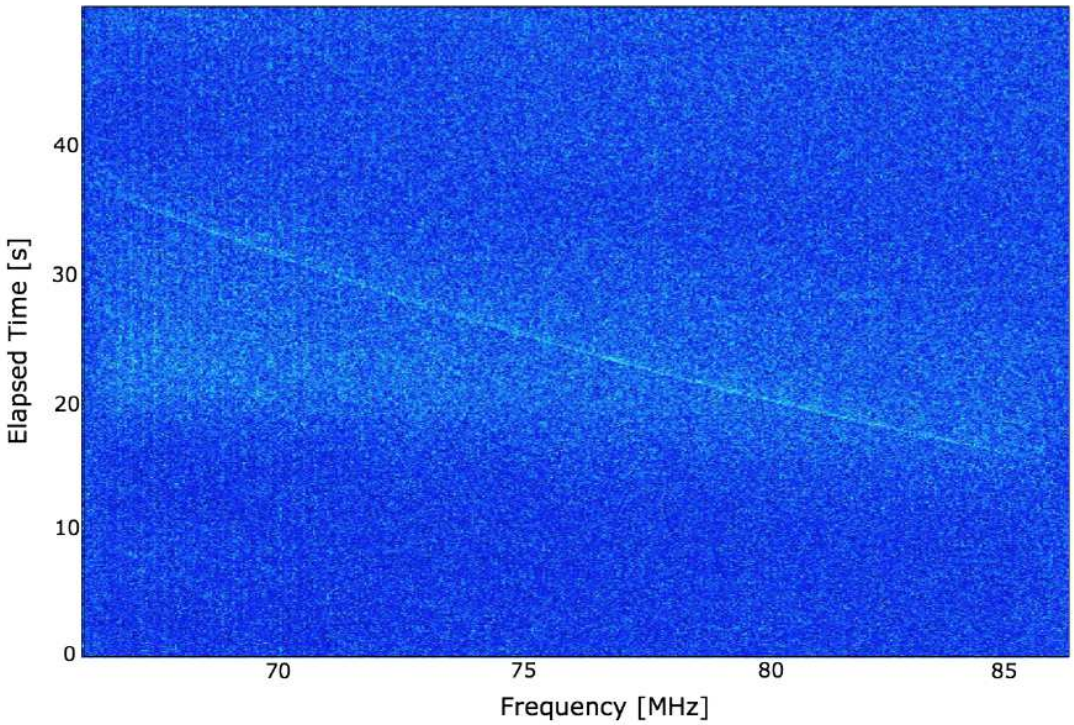

Figure 1. Illustration of the effect of dispersion on the signal from the Crab pulsar. The pulse is delayed for lower frequencies which results in a 'sweep' across the observing bandwidth. Figure from Eftekhari et al. (2016).

from the detector to the pulsar, $B_\parallel$:

$$RM = \frac{e^3}{2\pi m_e c^4} \int_0^L n_e B_\parallel ds, \tag{1}$$

where e is the electron charge, m_e is the electron mass, c is the speed of light in vacuum, and n_e is the electron density, with Gaussian units. The pulsar's DM can be expressed as $DM = \int_0^L n_e ds$. Thus, the weighted average magnetic field parallel to the line of sight is proportional to RM/DM.

This simple relation between magnetic field strength and RM and DM make pulsars indispensable for Galactic magnetic field measurements (Han 2013). Pulsar RMs were first exploited to measure Galactic magnetic fields by Manchester (1972) at 410 MHz. More recent measurements have been made by Han et al. (2006) and Noutsos et al. (2008) at 1.5 GHz with the Parkes Observatory. At lower frequencies the effect of Faraday rotation is greater, so RMs can be obtained with greater precision. Over many years as the pulsar moves through space, precise RMs can tell us about the variation in the magnetic field of the interstellar medium along the arc of sky that the pulsar travels.

Pulsars can be used to probe magnetic fields of objects other than the interstellar medium as well. Precision RMs obtained at long wavelengths can be used to find

the time-varying strength of the magnetic field of some object between the observer and the pulsar, such as the Sun, as long as the effects of the ionosphere are carefully corrected. The ionosphere is a layer of electrons above the Earth that varies on timescales on the order of a few minutes. In spite of this challenge, Howard et al. (2016) were able to use LWA1 to study a coronal mass ejection when PSR B0950+08 was about 5° from the Sun. It has also been proposed by Withers & Vogt (2017) to use pulsars similarly for planets, although the alignment would have to be very fortunate, and planets that emit strongly in radio such as Jupiter may overwhelm the pulsar signal.

Another reason to measure RMs in the long wavelength regime is to study the properties of pulsar emission. For example, it is routinely observed that linear and circular polarization tend to decrease at shorter wavelengths. One theory for this wavelength-dependent polarization property was put forth by von Hoensbroech et al. (1998), assuming a magnetosphere of cold, low-density plasma: the pulsar beam has orthogonal propagation modes that superpose due to birefringence and thus lose polarization at higher frequencies. This theory can be tested by comparing high and low frequency observations to see how linear and circular polarization changes (as in Noutsos et al. 2015).

RMs can also be used to calibrate ionospheric models; see, for example, Sotomayor-Beltran et al. (2013), in which the authors test their ionosphere modeling software by observing four pulsars with the Low-Frequency Array (LOFAR) at different times of day from widely-spaced stations within the array and with the higher-frequency Westerbork Synthesis Radio Telescope. Pulsar RMs are assumed to be constant over short timescales, so observations of a pulsar with a rotation measure known precisely from low-frequency observations can show the diurnal variation in the ionosphere.

The multitude of reasons to examine low-frequency pulsar polarization have motivated the recent studies of Johnston et al. (2008) at 243, 322 and 607 MHz with the Giant Metrewave Radio Telescope (GMRT), Noutsos et al. (2015) at 150 MHz with LOFAR, and Mitra et al. (2016) at 325 and 610 MHz with the GMRT. Using LWA1, we are able to complement these studies at observing frequencies between 10 and 88 MHz.

2. OBSERVATIONS

We observed with the LWA1 station (Taylor et al. 2012), a 256-antenna dipole array located on the Plains of San Agustin in New Mexico. The dipoles are arranged in a pseudo-random configuration with a diameter of 100m. LWA1 is able to observe with four independent beams simultaneously, and this beamforming capability was used for this project. Observations were performed between July 2015 and August 2016. Fifteen pulsars were observed with LWA1's beamforming mode for an hour each. Two beams were used to observe each source; each beam is split into two tunings centered on different frequencies. This produced observations in four frequency ranges with

a bandwidth of 19.6 MHz. The four tunings were centered at 35.1, 49.8, 64.5, and 79.8 MHz. The raw data was coherently de-dispersed and folded using the program DSPSR[1] (van Straten & Bailes 2011). Pulsars are routinely observed with LWA1 and de-dispersed data files are available to the public at the LWA Pulsar Data Archive[2]. For more information about LWA pulsar data, see Stovall et al. (2015).

Pulsars were selected for this study if they are particularly bright in the LWA frequency band or if there was evidence of polarization from a plot of Stokes' parameters. Polarization components are conveniently expressed in Stokes' parameters, which describe the polarization of light and can be used to find the circular and linear polarization of an observation. Stokes' parameters can also be used to find the polarization position angle, which is the orientation of the polarization plane. Stokes' parameters are defined as:

$$\begin{aligned} I &= E_x^2 + E_y^2 \\ Q &= E_x^2 - E_y^2 \\ U &= 2E_x E_y cos\phi \\ V &= 2E_x E_y sin\phi, \end{aligned} \tag{2}$$

where each E is an electric field component and ϕ is the phase between the x and y components of the field. These equations are for a linear feed, so they use the linear electric field components. I is the total intensity, V is the circular polarization, and linear polarization can be defined as a combination of linear components U and Q:

$$L = \sqrt{Q^2 + U^2} \tag{3}$$

and the polarization position angle is defined as:

$$\psi = \frac{1}{2} \arctan\left(\frac{U}{Q}\right). \tag{4}$$

Plots of Stokes' Q and U over the pulse period can indicate if a pulsar is polarized.

3. METHODS

Data reduction made use of PSRCHIVE (van Straten et al. 2012), a pulsar data analysis software package. Radio frequency interference (RFI) was removed using a median filtering algorithm and manually through visual inspection. The rotation measures were calculated using the method developed by Noutsos et al. (2008). The change in total linear polarization was calculated for 512-1024 trial RMs near the value obtained at higher observing frequency previously published in the ATNF Pulsar Database[3] (Manchester et al. 2005). The RM for each observation was found by fitting a Gaussian peak to the plot of linear polarization vs trial RM. We corrected

[1] http://dspsr.sourceforge.net/
[2] http://lda10g.alliance.unm.edu/PulsarArchive/
[3] http://www.atnf.csiro.au/people/pulsar/psrcat/

the linear polarization of the pulsar for the effect of the RM in order to produce polarization profiles. The effect of Faraday rotation through the ionosphere had to be subtracted to derive the galactic contribution to the RM. This was done using the model developed by Sotomayor-Beltran et al. (2013). Faraday rotation through the heliosphere was not accounted for, but this contribution is expected to be small because our observations were made at large angles from the Sun.

4. RESULTS

4.1. *Rotation Measures*

We were successful in obtaining a rotation measure in at least one frequency tuning for 15 pulsars. Table 1 lists the results as well as the period and DM of each pulsar. Cases where RMs were unable to be found in certain frequencies are usually because of lower sensitivity in the lowest frequency part of the band, depolarization at lower frequencies, or RFI in that band. Note that the uncorrected RM has typical errors of less than 0.03 rad/m^2, but the ionospheric correction that follows adds considerable uncertainty. Our results show the need for ionospheric modeling to improve so that the accuracy achieved by low-frequency observing is not lost. There is agreement between our results and those of Noutsos et al. (2015) and the other high-frequency observations published in the ATNF Pulsar Database.

Table 1. The results of the RM fitting process for 15 pulsars. The period is taken from the ATNF Pulsar Database and the DM is from Stovall et al. (2015). The frequency column lists the center frequency of the beam used for each observation. Column 5 contains the RM measurement taken directly from the observation while column 6 is the ionospheric RM at the time of observation. The rightmost column is the observed RM with the ionospheric RM subtracted.

Pulsar Name	Period (s)	DM ($cm^{-3}pc$)	Frequency (MHz)	RM $m^{-2}rad$)	Ionosphere RM ($m^{-2}rad$)	Corrected RM ($m^{-2}rad$)
B0628-28	1.2444	34.425(1)	49.8	46.67(5)	2.3(4)	44.4(4)
			64.5	46.676(6)		44.4(4)
			79.2	46.69(1)		44.4(4)
B0329+54	0.7145	26.779(1)	64.5	−63.776(4)	2.0(2)	-65.8(2)
			79.2	−63.780(4)		-65.8(2)
B0809+74	1.2922	5.771(2)	49.8	−13.33(1)	1.5(2)	-14.8(2)
			64.5	−13.35(3)		-14.8(2)
			79.2	−13.36(3)		-14.8(2)
B0823+26	0.5307	19.4789(2)	79.2	5.95(2)	1.3(2)	4.6(2)
B0834+06	1.2738	12.8640(4)	49.8	26.15(1)	1.6(2)	24.6(2)
			64.5	26.169(6)		24.6(2)
			79.2	26.129(4)		24.6(2)
B0919+06	0.4306	27.2986(5)	49.8	33.96(3)	1.3(2)	32.7(2)
			64.5	33.960(4)		32.7(2)
			79.2	33.90(2)		32.6(2)
B0943+10	1.0977	15.334(1)	64.5	16.07(2)	3.9(2)	12.2(2)
			79.2	16.3(2)		12.4(3)
B0950+08	0.2531	2.96927(8)	35.1	2.210(2)	1.5(2)	0.7(2)
			49.8	2.2111(4)		0.7(2)
			64.5	2.209(1)		0.7(2)
			79.2	2.215(3)		0.8(2)
B1133+16	1.1879	4.8480(2)	35.1	4.71(4)	1.2(2)	3.5(2)
			49.8	4.710(1)		3.5(2)
			64.5	4.713(3)		3.5(2)
			79.2	4.719(6)		3.5(2)
B1604-00	0.4218	10.6823(1)	35.1	7.13(4)	1.4(3)	5.7(3)
			49.8	7.115(3)		5.7(3)
			64.5	7.10(1)		5.7(3)

Table 1 continued on next page

Table 1 *(continued)*

Pulsar Name	Period (s)	DM ($cm^{-3}pc$)	Frequency (MHz)	RM $m^{-2}rad$	Ionosphere RM ($m^{-2}rad$)	Corrected RM ($m^{-2}rad$)
B1822-09	0.7690	19.3833(9)	79.2	68.9(3)	1.8(2)	67.1(3)
B1839+56	1.6529	26.774(1)	49.8	−3.25(2)	1.3(2)	-4.5(2)
			79.2	−3.3(1)		-4.6(2)
B1919+21	1.3373	12.4386(3)	64.5	−16.078(5)	1.4(2)	-17.4(2)
			79.2	−16.091(8)		-17.4(2)
B1929+10	0.2265	3.1828(5)	79.2	−6.5(5)[a]	3.4(2)	-9.9(5)
B2217+47	0.5385	43.4975(5)	64.5	−35.07(1)	1.2(2)	-36.3(2)
			79.2	−35.063(6)		-36.3(2)

[a]This error was estimated from visually inspecting the graph of trial rotation measure vs. linear polarization because Gaussian curve fitting failed.

4.2. *Average Magnetic Field*

The electron density weighted average magnetic field parallel to the line of sight can be expressed using RM and DM as defined in section 1:

$$\langle B_{\parallel} \rangle = \frac{\int_0^L n_e B_{\parallel} ds}{\int_0^L n_e ds} = \frac{2\pi m_e c^4}{e^3} \frac{RM}{DM}, \tag{5}$$

where the constants can be evaluated and expressed in the convenient units of cm^3 m^{-2} pc^{-1} μG^{-1} to match the standard units of RM and DM, resulting in a magnetic field in μG .

Table 2 shows the values we derived for $\langle B_{\parallel} \rangle$ from our RMs. This data is plotted in Galactic coordinates in figure 2. In the map, there is a trend of positive magnetic field (and rotation measure) for Galactic longitudes less than 30° and negative magnetic field for Galactic longitude greater than 30°. Our pulsars are relatively nearby, all within 3 kpc, and show the structure of the field local to the Sun. This region is thought to be in between the denser spiral arms of the Galaxy and has a clockwise magnetic field (Han et al. 2006). Our map is consistent with the work of Manchester (1972). It should be noted that clouds of ionized hydrogen in between the pulsar and Earth can confuse magnetic field measurements from pulsars (Mitra et al. 2003), but these clouds are fairly rare and are not expected to affect our measurements.

Table 2. A table showing the values of $\langle B_{\parallel} \rangle$ derived from the values of RM and DM in table 1. The values for distance, Galactic longitude (l), and Galactic latitude (b) are from the ATNF pulsar database.

Pulsar Name	Distance (kpc)	l (°)	b (°)	$\langle B_{\parallel} \rangle$ (μG)
B0628-28	0.32	-123.05	-16.76	1.59(1)
B0329+54	1.00	145.00	-1.22	−3.024(9)
B0809+74	0.43	140.00	31.62	−3.17(5)
B0823+26	0.32	-163.04	31.74	0.29(1)
B0834+06	0.19	-140.28	26.27	2.35(2)
B0919+06	1.10	-134.58	36.39	1.474(8)
B0943+10	0.89	-134.59	43.13	0.99(3)
B0950+08	0.26	-131.09	43.70	0.31(7)
B1133+16	0.35	-118.10	69.20	0.89(6)
B1604-00	0.68	10.72	35.47	0.66(3)
B1822-09	0.30	21.45	1.32	4.26(2)
B1839+56	2.19	86.08	23.82	−0.21(1)
B1919+21	0.30	55.78	3.50	−1.73(2)
B1929+10	0.31	47.38	-3.88	−3.8(2)
B2217+47	2.39	98.38	-7.60	−1.029(5)

4.3. *Polarized Pulse Profiles*

Using the RM to correct the linear polarization, we found a total of 36 pulse profiles. See appendix A for all plots. Each plot shows polarization in the bottom section, with black corresponding to total intensity, while red is linear polarization, and blue is circular polarization (Stokes' I, L, and V, respectively). Change in position angle (P.A.) in degrees vs. pulse phase is plotted in the top portion. For small fractional polarization (L/I< 0.3), the position angle is not plotted.

There are some interesting features that can be discerned from our low-frequency polarized profiles. As noted in section 1, some pulsar emission models predict depolarization at low frequencies, but for PSR B0950+08 we find an unusually high fraction of polarization in our frequency band. This pulsar is known to have an 'interpulse,' a small pulse far from the main pulse, at higher frequencies (Rickett & Lyne 1968), but we do not see the interpulse in our profiles. The unusual appearance of B0943+10 is because of its very weak polarization in our frequency band. PSRs B0823+26, B0834+06, and B1133+16 show an unusually high degree of circular polarization.

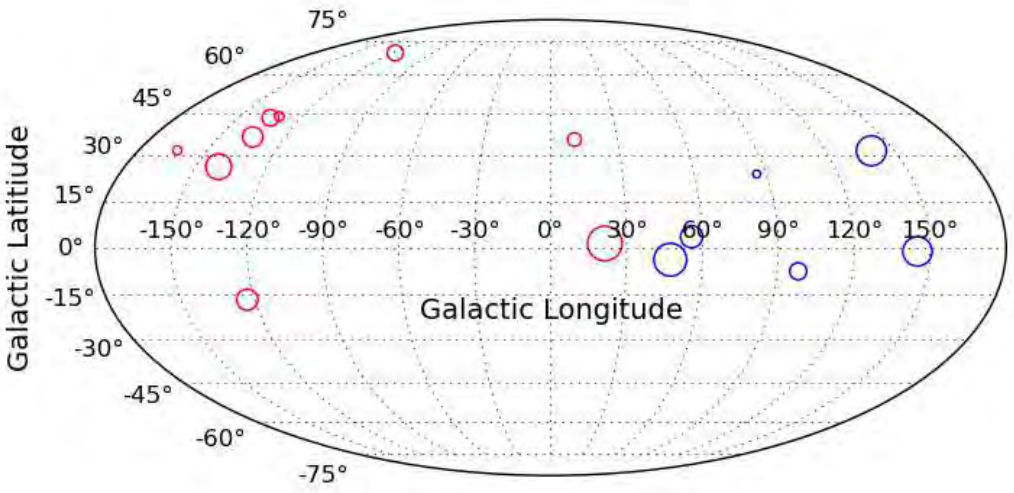

Figure 2. The derived Galactic magnetic field. Red circles correspond to a positive $\langle B_{\parallel} \rangle$, while blue corresponds to negative $\langle B_{\parallel} \rangle$. The size of the circles is proportional to the absolute value of the magnetic field strength, ranging from 0.21 μG to 4.26 μG.

Several profiles also have double peaks that change separation depending on frequency. In the interpretation of radius-to-frequency mapping (Ruderman & Sutherland 1975), which is the theory that different frequencies correspond to different emission heights above the pulsar, the peaks are thought to get farther apart at lower frequencies (higher emission heights). The usual widening can be seen in PSRs B0809+74, B0943+10, B0950+08, and B1133+16. However, PSR B919+21 does not obey this rule.

5. CONCLUSIONS

Using LWA1, we were able to obtain very precise rotation measures for 15 pulsars, although ionospheric effects reduced precision. Nevertheless, the technique has great promise for future applications in studies of the interstellar medium, the heliosphere, and pulsars themselves. We have used our rotation measures to show some features of the local Galactic magnetic field. We have presented 36 polarized profiles for 15 pulsars. These profiles extend our knowledge of the pulsar emission region to lower frequencies and higher emission heights than ever before.

REFERENCES

Baade, W., & Zwicky, F. 1934, Proceedings of the National Academy of Science, 20, 259

Eftekhari, T., Stovall, K., Dowell, J., Schinzel, F. K., & Taylor, G. B. 2016, ApJ, 829, 62

Han, J. 2013, in IAU Symposium, Vol. 291, Neutron Stars and Pulsars: Challenges and Opportunities after 80 years, ed. J. van Leeuwen, 223–228

Han, J. L., Manchester, R. N., Lyne, A. G., Qiao, G. J., & van Straten, W. 2006, ApJ, 642, 868

Hewish, A., Bell, S. J., Pilkington, J. D. H., Scott, P. F., & Collins, R. A. 1968, Nature, 217, 709

Howard, T. A., Stovall, K., Dowell, J., Taylor, G. B., & White, S. M. 2016, ApJ, 831, 208

Johnston, S., Karastergiou, A., Mitra, D., & Gupta, Y. 2008, MNRAS, 388, 261

Klochkov, D., Pühlhofer, G., Suleimanov, V., et al. 2013, A&A, 556, A41

Lyne, A. G., & Smith, F. G. 1968, Nature, 218, 124

Manchester, R. N. 1972, ApJ, 172, 43

Manchester, R. N., Hobbs, G. B., Teoh, A., & Hobbs, M. 2005, AJ, 129, 1993

Mitra, D., Basu, R., Maciesiak, K., et al. 2016, ApJ, 833, 28

Mitra, D., Wielebinski, R., Kramer, M., & Jessner, A. 2003, A&A, 398, 993

Noutsos, A., Johnston, S., Kramer, M., & Karastergiou, A. 2008, MNRAS, 386, 1881

Noutsos, A., Sobey, C., Kondratiev, V. I., et al. 2015, A&A, 576, A62

Rickett, B. J., & Lyne, A. G. 1968, Nature, 218, 934

Ruderman, M. A., & Sutherland, P. G. 1975, ApJ, 196, 51

Sotomayor-Beltran, C., Sobey, C., Hessels, J. W. T., et al. 2013, A&A, 552, A58

Stovall, K., Ray, P. S., Blythe, J., et al. 2015, ApJ, 808, 156

Taylor, G. B., Ellingson, S. W., Kassim, N. E., et al. 2012, Journal of Astronomical Instrumentation, 1, 1250004

van Straten, W., & Bailes, M. 2011, PASA, 28, 1

van Straten, W., Demorest, P., & Oslowski, S. 2012, Astronomical Research and Technology, 9, 237

von Hoensbroech, A., Lesch, H., & Kunzl, T. 1998, A&A, 336, 209

Withers, P., & Vogt, M. F. 2017, ApJ, 836, 114

Typeset using LaTeX **modern** style in AASTeX61

APPENDIX

A. POLARIZED PULSE PROFILE PLOTS

This appendix contains the plots of polarized pulse profiles and position angle rotation for all 15 pulsars. The upper portion of each plot shows the change in polarization position angle. Position angles are suppressed for low linear polarization fractions (L/I$<$ 0.3). The bottom portion of each plot shows pulse phase vs flux in arbitrary units. Black lines are total intensity, red is linear polarization, and blue is circular polarization.

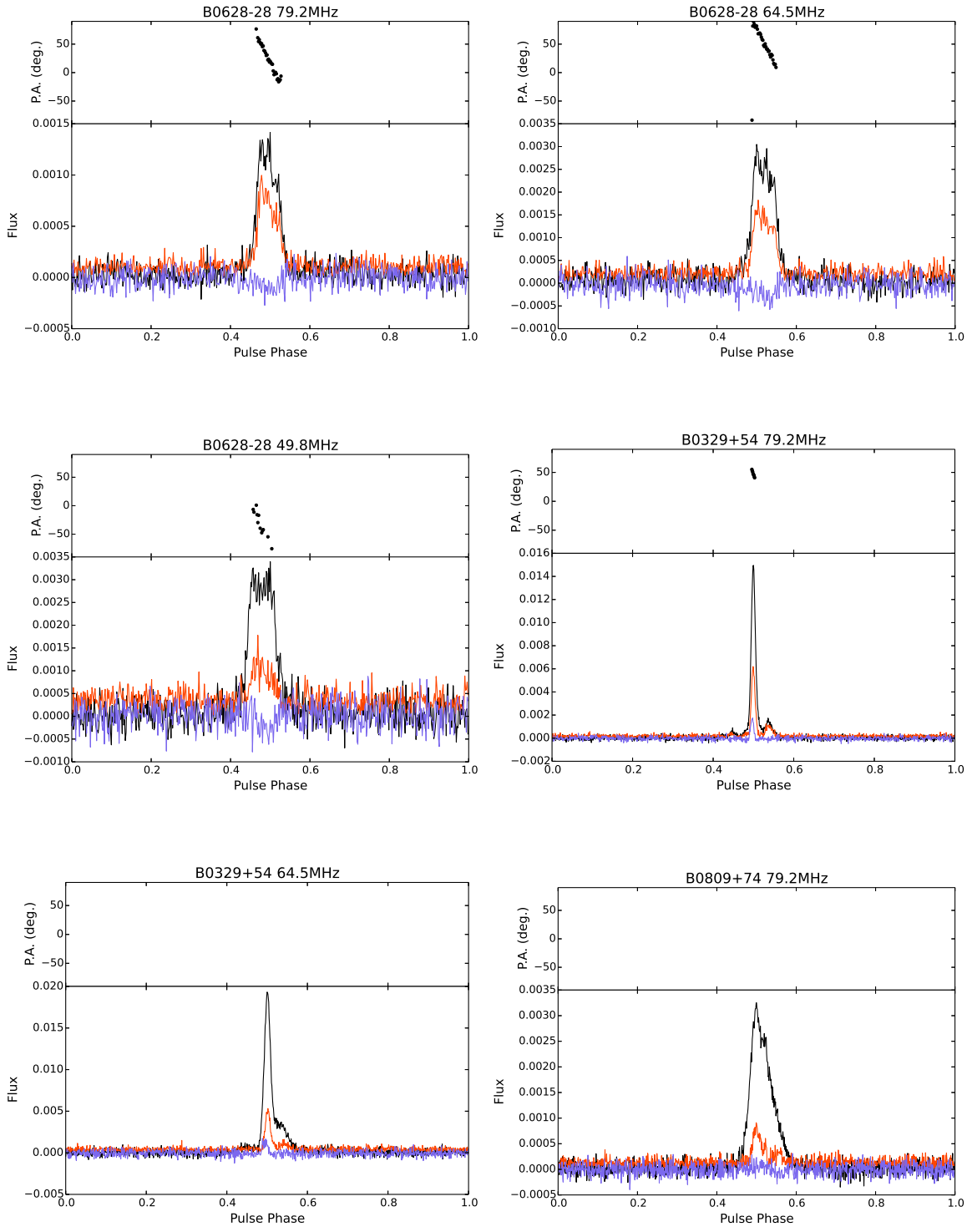

Figure A1. Profiles for B0628-28, B0329+54, and B0809+74.

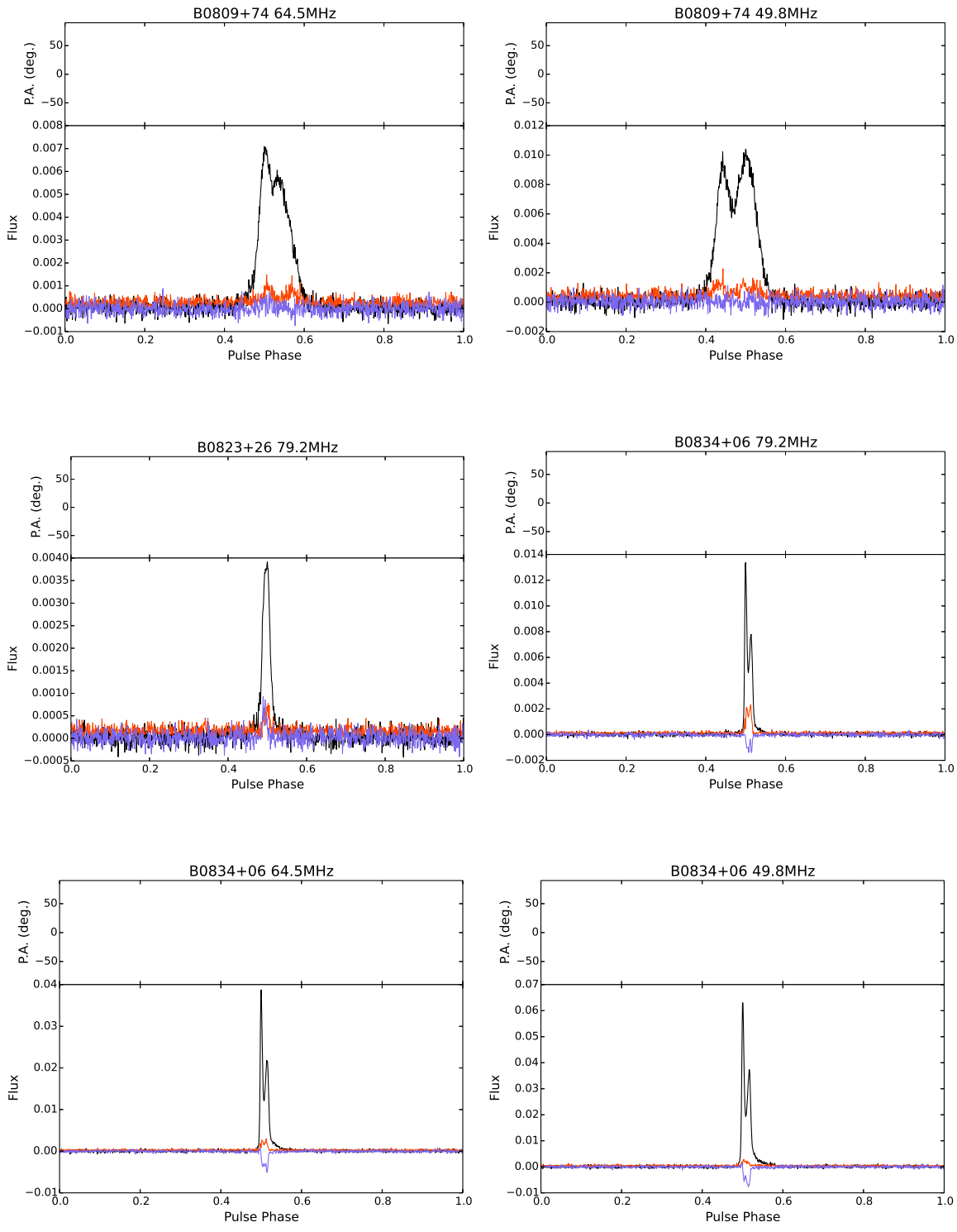

Figure A2. Profiles for B0809+74, B0823+26, and B0834+06.

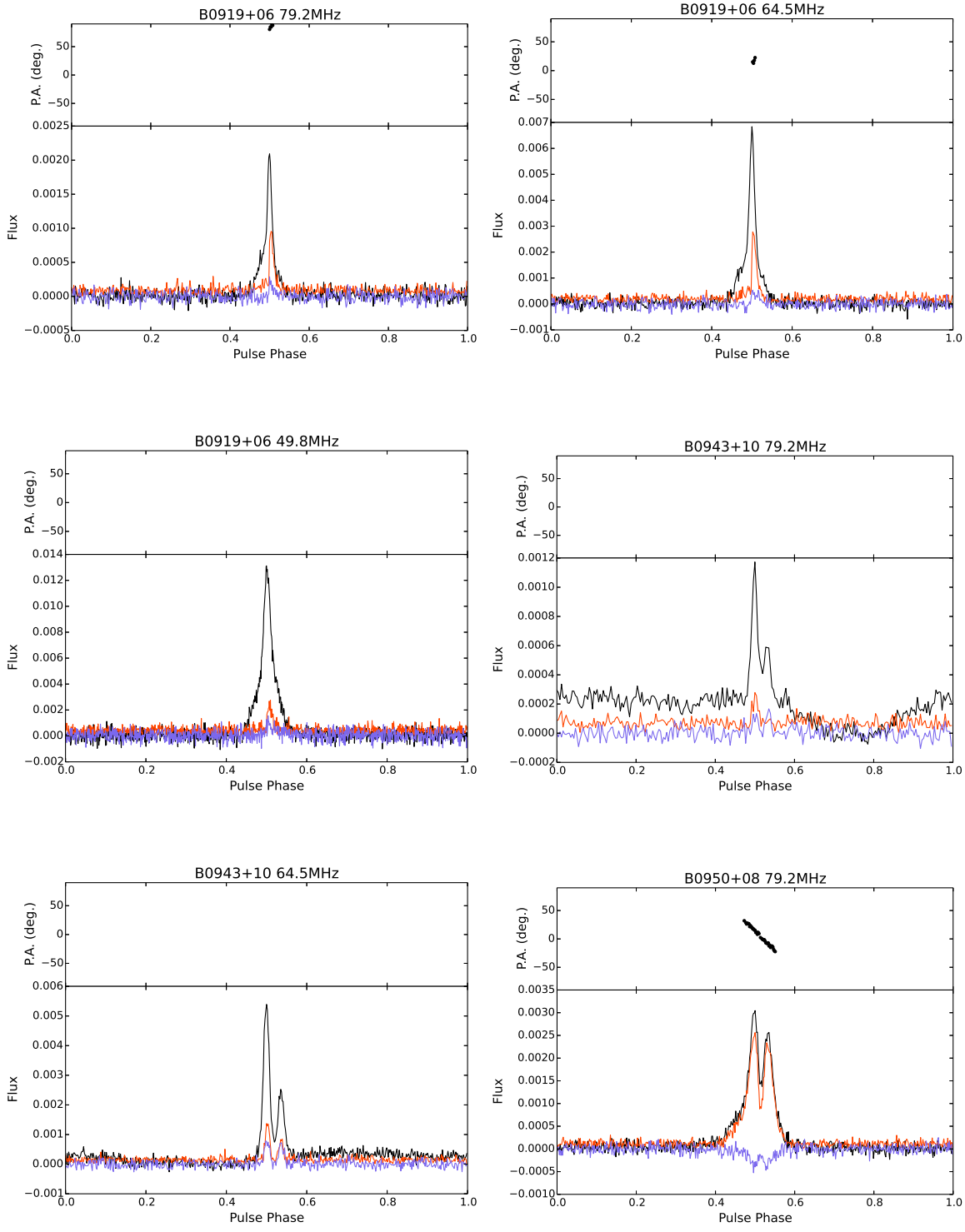

Figure A3. Profiles for B0919+06, B0943+10, and B0950+08 (continued on next page).

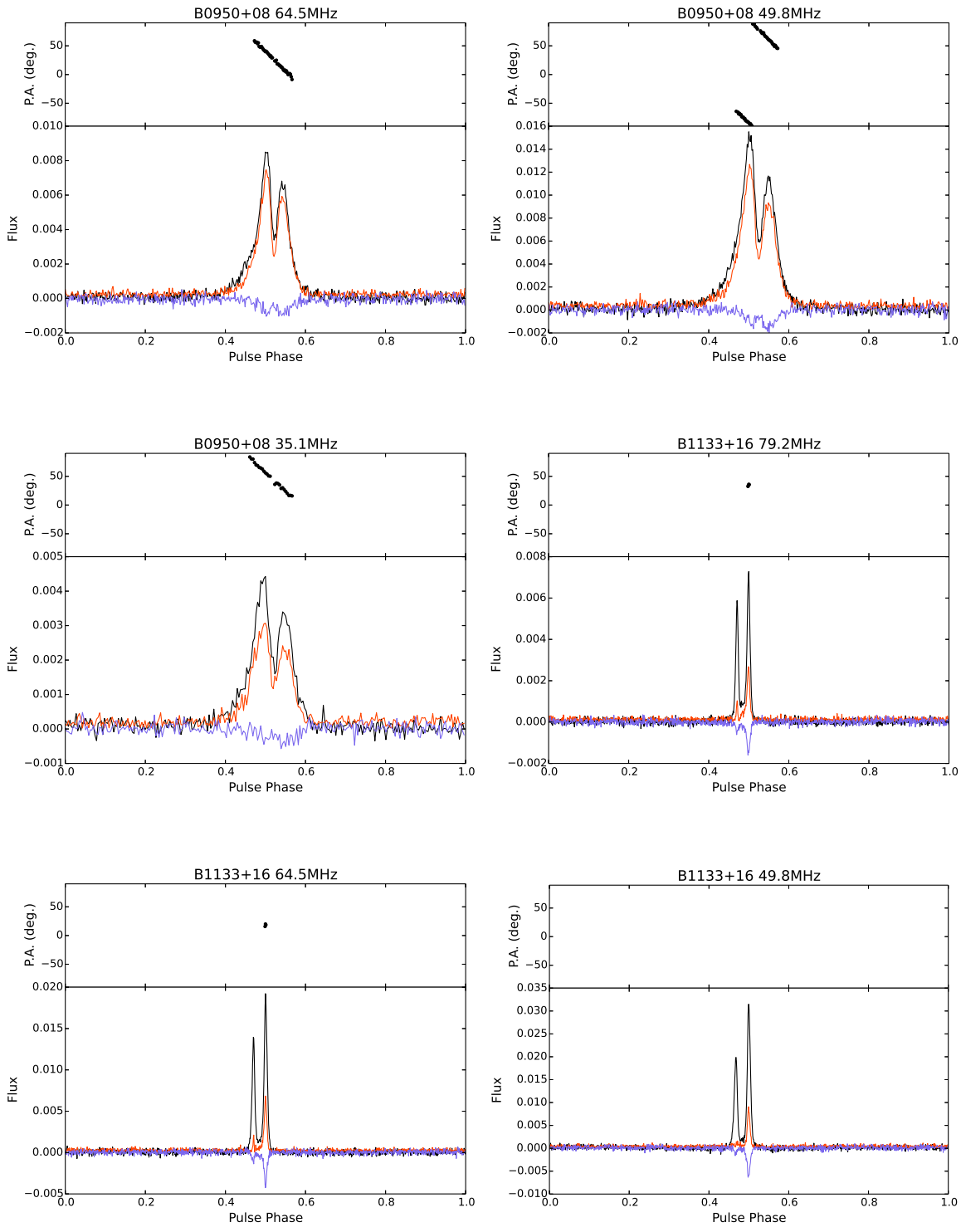

Figure A4. Profiles for B0950+08 (continued from last page) and B1133+16 (continued on next page).

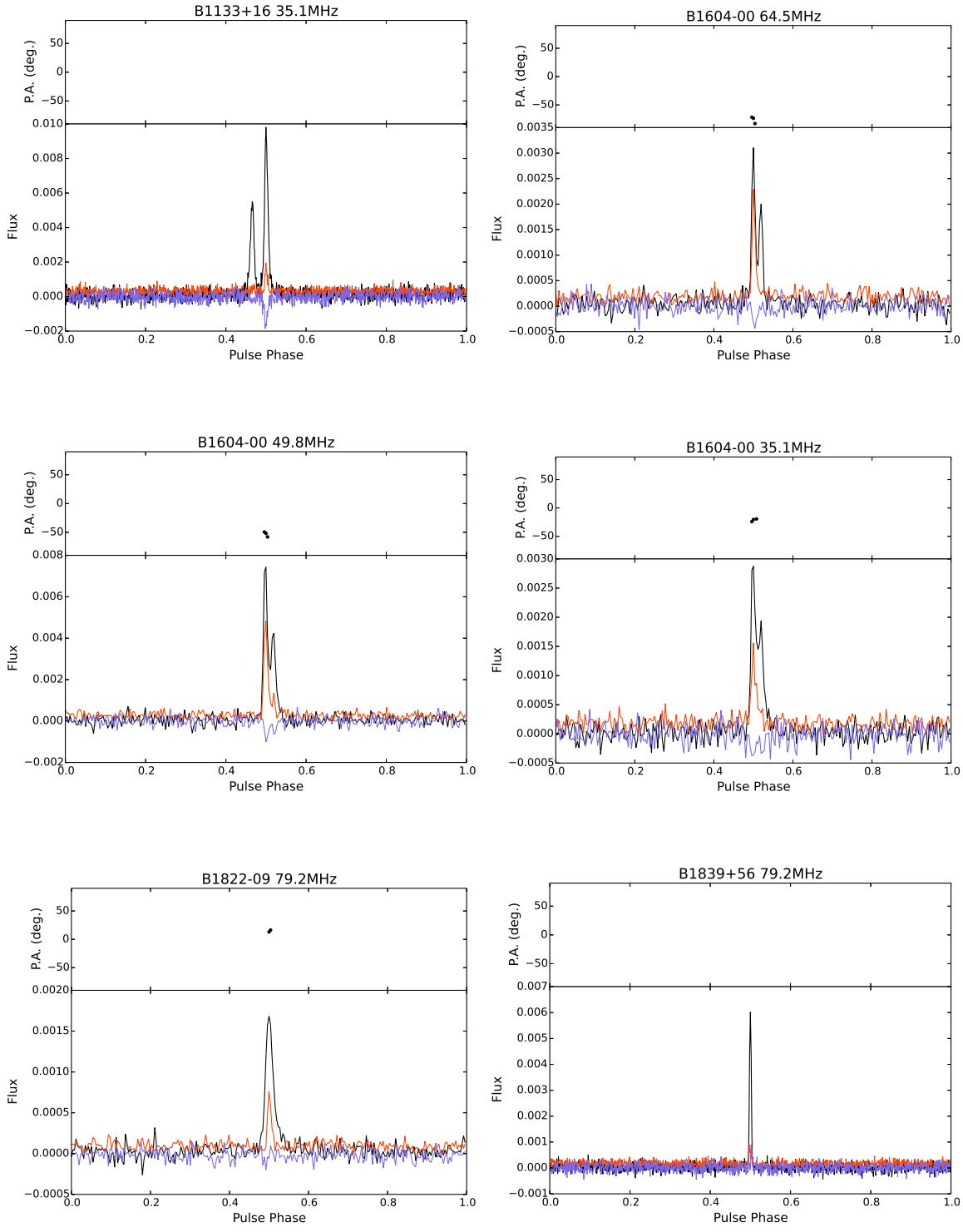

Figure A5. Profiles for B1133+16 (continued from last page), B1604-00, B1822-09, and B1839+56 (continued on next page).

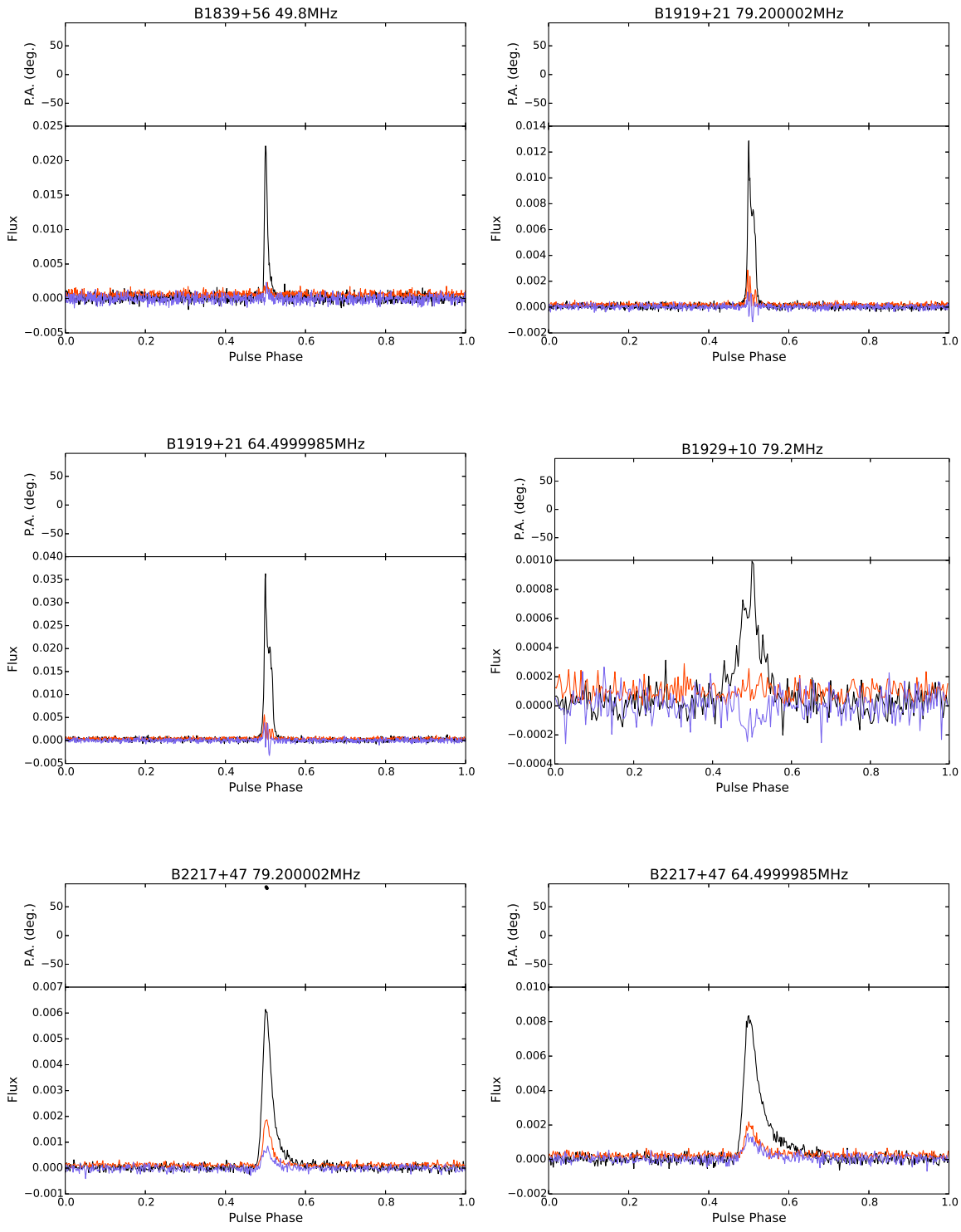

Figure A6. Profiles for B1839+56 (continued from last page), B1919+21, B1929+10, and B2217+47.